Microbiota–Muscle/–Immune Interactions in Rhesus Macaque under Simulated Weightlessness Revealed by Integrated Multi-Omics Analysis

Peng Zhang (zhangpeng6128@163.com)
China Astronaut Research and Training Center https://orcid.org/0000-0002-5835-4034
Libin Shao
BGI-Qingdao, BGI-Shenzhen
Jie Zhang
BGI-Qingdao, BGI-Shenzhen
Lu Wang
China Astronaut Research and Training Center
Huimei Yuan
China Astronaut Research and Training Center
Xiangsheng Pang
China Astronaut Research and Training Center
Guangyi Fan
BGI-Qingdao, BGI-Shenzhen
Ling Peng
BGI-Qingdao, BGI-Shenzhen
Guanghan Kan
China Astronaut Research and Training Center
Wenjiong Li
China Astronaut Research and Training Center
Xinming Liang
MGI, BGI-Shenzhen: BGI Group
Xin Liu
Beijing Genomics Institute Shenzhen: BGI Group
Xiaoping Chen
China Astronaut Research and Training Center

Short report

Keywords: Head-down tilted bed rest, Metagenomics, Microbiota, Metabolomics, Transcriptomic, Integrated multi-omics analysis

Posted Date: January 13th, 2021

DOI: https://doi.org/10.21203/rs.3.rs-142735/v1

Abstract

Background

Long-term exposure to microgravity during spaceflight has adverse effects on human health including muscle atrophy, impaired immune function, and alterations in gut microbiome profile. Gut microorganisms influence a wide range of host biological processes, but their interactions with skeletal muscle and the immune system under microgravity are not known.

Methods

Rhesus macaques (*Macaca mulatta*) were subjected to -6° head-down tilted bed rest (HDBR) for 6 weeks. Fecal samples, skeletal muscle tissue, and peripheral blood mononuclear cells (PBMCs) were collected for metagenomic, metabolomic, and transcriptomic analyses respectively and further integrated for a multi-omics analysis.

Results

HDBR resulted in significantly altered taxon abundance in 1 class, 5 orders, 11 families, 55 genera, and 122 species of microbes. We also identified the significantly changed metabolites in atrophied muscles, including some crucial metabolites (such as L-alanine and L-carnitine) and hub metabolites (such as pyridoxamine and epinephrine) involved in energy metabolism. Transcriptomic analysis of PBMCs revealed genes related to leukocyte activation, differentiation, and interleukin-2 production that were differentially expressed as a result of HDBR exposure. By integrating multi-omics analysis, we identified 3 bacterial genera (*Klebsiella*, *Kluyvera*, and *Bifidobacterium*) that were closely associated with immune dysfunction and 5 (including *Oligella*, *Sporosarcina*, *Citrobacter*, *Weissella*, and *Myroide*) that were associated with abnormal metabolism of amino acids in atrophied muscles induced by HDBR. Of note, the reduced abundance of butyrate-producing colon bacteria *Eubacterium*, *Roseburia* and their cross-feeding bacteria *Bifidobacteria* may contribute to both the impaired immune function and muscle atrophy caused by HDBR.

Conclusions

We first reported the HDBR-associated changes in gut microbiota composition, metabolomics of skeletal muscle and transcripts of PBMCs in non-human primate. Particularly, we revealed the underlying microbiota-muscle and microbiota-immune interactions during simulated microgravity, implicating that modulation of gut microbiota may represent a new strategy in enhancing crewmembers' health and safety during long-term space expeditions.

Background

The harsh environment of space poses a significant physiologic challenge to humans and has hindered the progress of deep space exploration. Astronauts experience a variety of pathophysiologic changes

during spaceflight such as space motion sickness [1], spatial disorientation [2], osteoporosis [3], muscle atrophy [4], and impaired cardiac [5, 6], cognitive [6, 7], and immune [8] functions. The operation of the International Space Station (ISS) further extended our knowledge of the effects of microgravity on human health. For example, many astronauts on the ISS reported ocular issues including optic disc edema, globe flattening, hyperopic shifts, and cotton-wool spots [9]. The National Aeronautics and Space Administration (NASA) twins study reported increased subfoveal choroidal thickness and peripapillary total retinal thickness [6]. Recently, a case of venous thromboembolism during spaceflight was also confirmed by radiologists on earth [10]. Generally, the physiological and functional alterations caused by spaceflight have been gradually well recognized.

Over the past two decades, a variety of high-throughput omics technologies such as methyl-CpG-binding domain protein sequencing [11], RNA sequencing [12], mass spectrometry (MS) analysis and metabolomics [13], have been used to investigate the impact of microgravity on human health. However, each omics technologies emphasize the role of molecules of their corresponding omic layer, but miss the complementary effects and interactions between omic layers [14]. Thus, an integrative approach to multi-omics data analysis is needed to fully elucidate microgravity-induced physiological changes.

The gastrointestinal tract harbors complex communities of microbes that play important roles in maintaining human health, including energy extraction, vitamin biosynthesis, protection against pathogens, and development of the innate and adaptive immune systems [15, 16]. Although changes in the gut microbiome profile in response to microgravity have been reported in both human and rodents [6, 17], how these relate to other microgravity-induced pathophysiologic alterations is unclear. To address this point, we carried out an integrative multi-omics analysis covering metagenomics of fecal samples, metabolomics of skeletal muscle and transcripts of peripheral blood mononuclear cells (PBMCs) from rhesus macaques subjected to -6° head-down tilted bed rest (HDBR). The multi-omics dataset generated in this study can serve as a resource for future investigations on the effects of microgravity on human health and may guide the development of potential countermeasures for future spaceflights.

Material And Methods

Animal experiments

A total of 15 healthy male rhesus macaques aged 4–6 years and weighing 4–8 kg were provided by the Beijing Institute of Xie'erxin Biology Resource (Beijing, China). The animals were acclimatized for 3 months at the Laboratory Animal Center of China Astronaut Research and Training Center prior to being used in experiments. Ultimately, 5 fully acclimatized rhesus macaques were included in the study and subjected to 42 days of -6° HDBR as previously described [18]. After the treatment, the animals were individually housed in stainless steel mesh cages where they were allowed to recover for 32 days. The animals had free access to food and water and their general health condition was closely monitored for the duration of the study.

Sample collection

All biological samples were collected according to protocols approved by the Beijing Genomics Institute (BGI) Ethics Committee. Under light ketamine sedation, sterile heparinized peripheral blood samples were obtained from the femoral vein of rhesus macaques before (Pre-3), during (H + 25 and H + 40), and after (R + 12, R + 24, and R + 32) HDBR at 10:00 a.m. PBMCs were collected by Ficoll-Hypaque density gradient centrifugation. Fecal samples were also collected from rhesus macaques before (Pre-2), during (H + 16, H + 30, and H + 42), and after (R + 13, R + 17, and R + 28) HDBR (Additional file 1: Figure S1).

Muscle biopsy

Muscle tissue samples were obtained by biopsy as previously described [19]. Briefly, after general anesthesia with isoflurane, the pre-HDBR muscle tissue sample (Pre-3) was obtained from the left soleus of rhesus macaques using an open biopsy technique. At the end of HDBR (H + 42), a biopsy was performed on the right soleus; and 32 days after HDBR, when the pre-HDBR biopsy site in the left soleus was fully healed, the muscle was biopsied at a different site (R + 32) (Additional file 1: Figure S1). All muscle samples were immediately frozen in liquid nitrogen after biopsy until use.

Transcriptome analysis

Total mRNA of PBMCs was amplified using oligo (dT) primers and sequenced by Complete Genomics (San Jose, CA, USA). At least 20 million reads were generated for each sample, and SOAPnuke was used to filter out those of low quality [20]. HISAT2 was used to map sequence reads to the reference genome and RNA-Seq by Expectation Maximization was used to calculate fragments per kilobase million (FPKM) [21]. Spearman correlations between all samples were calculated based on FPKM and were found to be very high (> 0.95) and biological replicates clustered well together. We used DESeq2 package in R to identify differentially expressed genes (DEGs), and performed Gene Ontology (GO) analysis for functional annotation [22].

Metabolome analysis

Metabolite detection was carried out by ultrahigh-performance liquid chromatography (UPLC)-MS. Quality control samples were included to evaluate data quality, and low-quality samples were removed. Feature alignment, picking, and identification were performed using Progenesis QI software (Nonlinear Dynamics, Newcastle, UK). MetaX software was used for data cleaning and statistical analysis [23]. Significantly altered features ($P < 0.05$, fold change < 1/1.2 or > 1.2, and variable importance in projection [VIP] > 1) were identified by combining uni- and multivariate analyses and annotated using Progenesis QI and the Human Metabolome Database (HMDB) v.3.6 and Kyoto Encyclopedia of Genes and Genomes (KEGG) database (www.genome.jp/kegg/) [24].

Clusters of co-abundant metabolites in muscle tissue were identified by weighted gene correlation network analysis (WGCNA) in R package [25]. A soft threshold of $\beta = 9$ for muscle features was selected by scale-free topology analysis for signed, weighted features co-abundance correlation network construction. A dynamic hybrid tree-cutting algorithm with deepSplit = 4 and a minimum cluster size of 30

was used for cluster identification. If the biweight mid-correlation between 2 clusters' eigenvectors was > 0.8, they were considered similar and were merged. Muscle feature clusters were labeled as M1–M6.

Metagenome analysis

Raw reads sequenced on the Illumina HiSeq 2000 platform (Expression Analysis, San Diego, CA, USA) at BGI were filtered to remove adapter contamination, low-quality reads, and host genomic DNA (rhesus macaque, assembly Mmul_8.0.1, National Center for Biotechnology Information [NCBI]). The remaining high-quality reads were assembled using metaSPAdes v.3.10.1 [26]. Open reading frames (ORFs) in contigs of each sample were determined using GeneMark v.2.7 [27]. The nonredundant gene set of all ORFs was clustered using CD-HIT v.4.5.7 based on the nucleotide sequence with thresholds of 95% identity and 90% coverage [28]. Taxonomic annotation of gene sets was carried out using CARMA3 based on BLASTP alignment with bacteria and archaea genes from the NCBI-NR database [29]. The gene set was also annotated against the KEGG v.59 database using BLAST v.2.2.23.

Gene abundance was calculated based on SOAP2 alignment and species abundance and functional profiles were summarized from their respective genes [30]. The differential alpha diversity, species, and KEGG orthologs (KOs) at different time points were calculated with the Kruskal–Wallis test using R software (https://www.r-project.org/). Spearman's correlation coefficient was used to evaluate the relationship between different genera and KOs or metabolic features according to their abundance.

Results

HDBR-associated changes in gut microbiome profile

To investigate the effect of HDBR on the gut microbiome, we carried out metagenome sequencing of 35 gut samples of rhesus macaque collected at 7 time points throughout the whole experiment (Additional file 1: Figure S1). A total of 286.86 Gb of raw data were generated; after removing low-quality and host reads, 275.99 Gb of high-quality data were obtained (average of 7.89 Gb per sample) (Additional file 2: Table S1). We constructed a reference library of the rhesus macaque gut metagenome using all of the samples (Additional file 3: Table S2); 63.10%, 21.00%, and 2.43% of the genes were annotated at the phylum, genus, and species levels, respectively, and 45.51% were annotated to 6631 KOs. *Firmicutes* and *Bacteroidetes* were the predominant phyla while *Prevotella* and *Clostridium* were the predominant genera (Fig. 1A, B). Genes related to metabolism constituted the largest proportion of total genes in the KEGG pathway analysis (Fig. 1C). 95.58% of KO functions and 49.48% of genera were shared between rhesus macaque and human gut gene catalogs (Additional file 4: Figure S2).

To identify microbial taxa affected by spaceflight, we compared pre-HDBR (control) and HDBR as well as HDBR and post-HDBR (recovery) gut microbiome profiles with the Kruskal–Wallis test. A number of bacterial taxa were significantly different between control and HDBR samples (1 class, 5 orders, 11 families, 55 genera, and 122 species), and some of these showed the reverse trend during recovery period (1 class, 1/5 orders, 3/11 families, 24/55 genera, and 72/122 species) (Additional file 5: Table S3). For

example, the abundance of *Acinetobacter* and *Lactococcus*, two genera involved in the regulation of inflammation and protection against infections, was decreased by HDBR but returned to the baseline (pre-HDBR) level after 17 days of recovery (Fig. 2A). However, the abundance of some genera was not restored even after 28 days of recovery; for example, the level of *Bifidobacterium*, a beneficial gut bacterium, decreased continuously throughout the experiment (Fig. 2A).

We also identified 537 KOs with significantly altered abundance assigned to 139 genera, of which 27 were significantly altered throughout the experiment ($P < 0.05$). A correlation analysis showed that 44.76% of pairwise correlations between KOs and specific genera were positive while 3.38% were negative ($R^2 > 0.3$, $P < 0.05$) (Fig. 2B). For example, a higher abundance of *Myroides* and *Acinetobacter* was associated with increased representation of K00121, K00151, K00276, K00451, and K01555, which are involved in tyrosine metabolism, indicating that changes in the abundance of specific genera are associated with altered gut microbial function during HDBR.

Metabolic profile associated with HDBR in skeletal muscle

To investigate the metabolic signature associated with HDBR in greater detail, we carried out a UPLC–MS-based metabolomic analysis to quantify metabolites in skeletal muscle tissue of rhesus macaque before, during, and after HDBR (Additional file 1: Figure S1 and Additional file 6: Table S4). We identified 356, 287, and 100 differentially abundant features (DAFs) in the HDBR vs control, HDBR vs recovery, and recovery vs control comparisons, respectively ($P < 0.05$, fold change > 1.2, VIP > 1) (Additional file 7: Figure S3A). We focused on the 154 DAFs that were significantly altered in HDBR relative to the control and recovery samples ($P < 0.05$) (Additional file 7: Figure S3B). In the KEGG pathway analysis, the top 5 most affected pathways were tyrosine metabolism; biosynthesis of amino acids; protein digestion and absorption; alanine, aspartate, and glutamate metabolism; and tryptophan, consistent with accelerated protein degradation occurring in HDBR-induced muscle atrophy (Additional file 8: Table S5).

In addition, the interaction of these DAFs was evaluated by WGCNA. We classified 552 DAFs in muscle into 6 modules (Fig. 3A). DAFs involved in tyrosine metabolism (mcc00350) were mainly distributed into 3 modules (M1, M5, and M6) (Fig. 3B, C). DAFs in M1 showed co-abundance in muscle that the levels of all of these metabolites were decreased during HDBR but were reversed in the recovery group (Fig. 3D, E). Consistent with the known metabolic and functional changes in skeletal muscle under microgravity, the DAFs in M1 contained some critical amino acids involved in gluconeogenesis (eg, L-alanine [KEGG compound C00041, HMDB00161]) and fatty acid transport (eg, L-carnitine [C00318, HMDB00062]) (Fig. 3F). Notably, we identified epinephrine (C00788, HMDB00068) as the hub metabolite of M1 (Fig. 3G). Pyridoxamine (C00534, HMDB01431), a form of vitamin B6 that participates in free radical scavenging, was identified as the hub metabolite of M6 (Fig. 3G).

Transcriptional signature associated with HDBR in PBMCs

We collected PBMCs from 5 rhesus macaques throughout the experiment to evaluate the effect of HDBR on gene expression in immune cells (Additional file 1: Figure S1). A total of 779.09 Mb reads were

obtained at 6 time points (Additional file 9: Table S6). By comparing every two time points (fold change > 2 and $P < 0.05$) and removing duplicate genes, we detected 65 DEGs (Additional file 10: Figure S4A) that were significantly enriched in 44 biological processes ($P < 0.05$); 41 were related to immune regulation including leukocyte activation (GO:0002694), T cell differentiation (GO:0045580), and interleukin (IL)-2 production (GO:0032663) (Additional file 10: Figure S4B and Additional file 11: Table S7). DEGs associated with these biological processes were mainly downregulated by HDBR, which is consistent with previous findings that immune function was impaired by simulated or actual microgravity [8, 31].

Integrated analysis of -omics data

To clarify the functional implications of microgravity-associated changes in gut microbiome profile, we performed a multi-omic analysis of combined metagenomic, transcriptomic, and metabolomic data from fecal samples, PBMCs, and muscle tissue, respectively. As shown in Fig. 4, 16 of the 27 genera that were differentially represented in fecal samples during HDBR were closely associated with 27 of the 65 DEGs in PBMCs, with *Klebsiella*, *Kluyvera*, and *Bifidobacterium* showing the highest correlations. More specifically, *Bifidobacterium* abundance was positively correlated with the expression of ENSMMUG00000015297 (cluster of differentiation [CD]69), ENSMMUG00000045565 (DNA damage-inducible transcript [DDIT]4), ENSMMUG00000010956 (suppressor of cytokine signaling [SOCS]1), ENSMMUG00000008869 (TNF alpha-induced protein [TNFAIP]3), and ENSMMUG00000011607 (nuclear receptor subfamily 4 group A member [NR4A]2) and negatively correlated with ENSMMUG00000005738 (N-acetyltransferase [NAT]9) and ENSMMUG00000005325 (solute carrier family 5 member 10 [SLC5A]10). Some intestinal bacteria were associated with specific gene in host PBMCs. For example, the abundance of *Delftia*, *Stenotrophomonas*, *Acinetobacter*, and *Comamonas* was positively correlated with ENSMMUG00000038412 (docosahexaenoic acid omega-hydroxylase CYP4F3, LOC718349) and negatively correlated with ENSMMUG00000010256 (early growth response [EGR]2) and ENSMMUG00000008817 (zinc finger protein [ZNF]441).

By integrating metagenomic data from fecal samples and metabolomic data from atrophied muscle, we found that 25 of the 27 differentially represented genera were closely correlated with 174 of 372 differentially expressed metabolites in muscle (Fig. 5), with *Oligella*, *Sporosarcina*, *Citrobacter*, *Weissella*, and *Myroide* showing the highest correlations. Notably, the abundance of *Oligella* was positively correlated with up to 45 metabolites and negatively correlated with 12 metabolites; and that of *Myroide* was negatively correlated with leucodopachrome (C05604, HMDB04067) and dopaquinone (C00822, HMDB01229), which are involved in tyrosine metabolism (mcc00350). Some bacterial genera were closely correlated with crucial metabolites identified in HDBR-induced muscle atrophy. For example, the abundance of *Oligella* was positively correlated whereas that of *Citrobacter* was negatively correlated with l-alanine; *Lactococcus* showed a positive correlation with L-carnitine; and *Providencia* was positively correlated with p-cresol (C01468, HMDB01858), a metabolite of tyrosine (Fig. 5).

Microbiota-derived short-chain fatty acids (SCFAs) are thought to mediate interactions between gut bacteria and other tissues [32, 33]. For example, butyrate-a major SCFA produced by these

microorganisms-prevents excessive inflammation by stimulating the function of M2 macrophages and regulatory T cells and inhibiting neutrophil infiltration [34]; moreover, administration of butyrate was shown to increase muscle mass and cross-sectional area in aged mice [35]. The abundance of butyrate-producing colon bacteria such as *Eubacterium* and *Roseburia* spp. and their cross-feeding bacteria *Bifidobacterium* was reduced during HDBR, suggesting that a lower level of butyrate may contribute at least in part to the impaired immune function and muscle atrophy caused by HDBR (Additional file 12: Figure S5). 3-Hydroxyphenylacetate can be transformed into 3,4-dihydroxybenzeneacetic acid (3,4DPHAA; C01161, HMDB01336)-a metabolite involved in tyrosine metabolism in skeletal muscle-by the enzyme 4-hydroxyphenylacetate 3-monooxygenase (EC: 1.14.14.9), which is produced by *Providencia rettgeri*. 3,4DPHAA level was increased during HDBR and returned to the baseline level during the recovery phase, reflecting the changes in *P. rettgeri* abundance in the gut and suggesting that this bacterium influences tyrosine metabolism in HDBR-induced muscle atrophy via 3,4DPHAA (Additional file 12: Figure S5). Besides, tryptophan 2,3-dioxygenase (EC: 1.13.11.11) produces N'-formylkynurenine (C02700, HMDB60485); which is transformed into formylanthranilic acid (C05653, HMDB04089) involved in tryptophan metabolism by kynureninase (EC: 3.7.1.3). Both tryptophan 2,3-dioxygenase and kynureninase are produced by gut microbes, such as *Myroides* and *Comamonas*, that showed significant changes in abundance during HDBR (Additional file 12: Figure S5). Collectively, these findings indicate that changes in microbiota community composition influence amino acid metabolism in skeletal muscle as well as immune function in rhesus macaque exposed to HDBR.

Discussion

It is well established that long-term spaceflight results in a broad spectrum of deleterious effects on human health. For example, the homeostasis of intestinal microbiota had been reported to be disturbed both in humans and rodents exposed to microgravity [6, 17], however, the former human study involved only a single set of twins, while the findings of the latter were not fully applicable to humans because of interspecies physiologic differences. Given the limited availability of biological samples from astronauts, more animal studies-especially in nonhuman primates-are needed to clarify the impact of microgravity on physiologic functions in mammals. In this study, we performed a longitudinal analysis of changes in the gut microbiome in response to HDBR. Consistent with the findings from the NASA twins study [36, 37], microgravity induced a decrease in the abundance of beneficial gut bacteria such as *Bifidobacterium* and an increase in that of opportunistic pathogens such as *Escherichia coli*; the lower abundance of *Bifidobacterium* during HDBR was also observed in fecal samples and continued to decrease during the 28-day recovery period. However, HDBR does not fully simulate the environmental conditions encountered during spaceflight and has relatively modest effects on the gut microbiome. HDBR caused no changes at the phylum level, and only 1 class showed differential abundance in fecal samples of rhesus macaque. In contrast, a 1-year spaceflight altered the abundance of 3 phyla and 3 classes of bacteria in the fecal microbiome of astronauts. Surprisingly, HDBR in rhesus macaque produced more differentially abundant families (11 vs 8), genera (55 vs 13), and species (122 vs 36) than did microgravity in humans. Given that microbiota community composition is strongly influenced by diverse factors such as diet, lifestyle, and

medication use, we speculate that the specific diet and nutritional supplementation for astronauts may alleviate the negative effects of microgravity on gut microbiome composition, especially from family level to species level.

In addition to nutrient absorption, intestinal microorganisms maintain human health through bidirectional interactions with host biological processes including the immune system [38, 39]. Studies in pathogen-free or gnotobiotic animals have demonstrated that the intestinal immune system influences the compartmentalization of commensal microbiota and microbial community composition; reciprocally, gut bacteria affect the development of organized lymphoid structures and intestinal and systemic immune cell function [38, 39]. In this study, HDBR reduced the abundance of butyrate-producing colon bacteria including *Eubacterium*, *Roseburia*, and *Bifidobacterium*. The SCFA butyrate is believed to mediate communication between commensal bacteria and the immune system [33]. It suppresses the production of proinflammatory cytokines released by M1 macrophages and neutrophils while activating Tregs, stimulating the production of the anti-inflammatory cytokine IL-10, and increasing the expression of interferon (IFN)-γ and granzyme B in cytotoxic T lymphocytes and Tc17 cells [34, 40]. As simulated or actual microgravity can weaken immune function and increase susceptibility to infection as a result of reduced lymphocyte proliferation and IFN-γ production [8], the reduced abundance of butyrate-producing microbiota may contribute to the immune dysfunction caused by HDBR. Besides *Bifidobacterium*, we also found that *Klebsiella* and *Kluyvera* were closely associated with immune dysfunction. *Klebsiella* species causes infections such as pneumonia, urinary tract infections (UTIs), bloodstream infections, and sepsis [41]; and *Kluyvera* is a potentially pathogen that infects hosts under various conditions [42]. It remains to be determined how changes in the abundance of these two genera influence host susceptibility to infection.

The relationship between intestinal microbiota community composition and skeletal muscle has recently been investigated [43, 44]. Reduced muscle mass was shown to be closely correlated with a specific gut microbiome signature [43–45]. For example, muscle atrophy in ghrelin-null mice was accompanied by selective depletion of butyrate-producing bacteria such as *Clostridium* XIVa and *Roseburia* [44], and there is evidence for an association between frailty and reduced abundance of butyrate-producing bacteria [46]. The administration of probiotics such as *Lactobacillus reuteri* and *Faecalibacterium* has been shown to alleviate the loss of muscle mass [47–49]. Butyrate treatment was also found to increase muscle mass and cross-sectional area in aged mice [35]. Based on these previous findings, it is reasonable to come to the conclusion that muscle atrophy caused by HDBR can be partly attributed to the reduced abundance of butyrate-producing bacteria. Five other bacterial genera (*Oligella*, *Sporosarcina*, *Citrobacter*, *Weissella*, and *Myroide*) that have been mainly implicated in UTIs were closely related to abnormal metabolism of amino acids in HDBR-induced muscle atrophy, although the mechanistic basis for this association is unclear. We speculate that intestinal mucosal barrier disruption and enhanced intestinal permeability under microgravity results in the release of LPS and proinflammatory cytokines by these pathogens, which may promote muscle atrophy [36]. Supporting this possibility, bacteria-derived indoxyl sulfate was reported to enhance the expression of myostatin and atrogin-1 in atrophic skeletal muscle [50].

Conclusions

In summary, we described microbiota–immune/–muscle interactions in rhesus macaque under simulated microgravity using a multi-omics approach. Despite the phylogenetic proximity, our results may not be completely recapitulated in human. Nevertheless, our research has extended our understanding of the effects of gut microbiota on host physiology under microgravity and provided us with a new strategy to enhance astronauts' adaptation in space, for instance, increasing the abundance of butyrate-producing microorganisms in the intestine during space missions through dietary supplementation.

Abbreviations

CNSA: China Nucleotide Sequence Archive; DAFs: Different abundance features; DDIT4: DNA damage inducible transcript 4; DEGs: Differential expressed genes; EGR2: Early growth response 2; HDBR: Head-down tilted bed rest; ISS: International Space Station; IL: interleukin; KOs: KEGG Orthologs; MAD: Median absolute deviation; NASA: National Aeronautics and Space Administration; NAT9: N-acetyltransferase 9; NR4A2: Nuclear receptor subfamily 4 group A member 2; PBMCs: Peripheral blood mononuclear cells; RNA-seq: RNA sequencing; SCFAs: Short-chain fatty acids; SOCS1: Suppressor of cytokine signaling 1; TNF alpha induced protein 3, TNFAIP3 SLC5A10: Solute carrier family 5 member 10; UPLC/MS: Ultra-performance liquid chromatography/mass spectrometry; UTIs: Urinary tract infections; WGCNA: Weighted correlation network analysis; ZNF441: Zinc finger protein 441;

Declarations

Ethics approval and consent to participate

All procedures were performed in accordance with the principles of the Association for Assessment and Accreditation of Laboratory Animal Care International (AAALAC) and the National Institutes of Health guide for the care and use of Laboratory animals (NIH Publications No. 8023, revised 1978), approved by Institutional Animal Care and Use Committee of China Astronaut Research and Training Center (ACC-IACUC-2014-001).

Consent for publication

Not applicable

Availability of data and materials

All data analyzed in this study are included in this published article and its supplementary information files. The metagenomics data of fecal samples, and transcriptomic data of peripheral blood mononuclear cells (PBMCs) generated and/or analysed during the current study are available in the China Nucleotide Sequence Archive (CNSA) databases under the following accession numbers: CNP0000147 (https://db.cngb.org/search/?q=CNP0000147). The main scripts of this article have been deposited in

https://pan.genomics.cn/ucdisk/s/3AVNj2. The metabolomics data of skeletal muscle is available at https://pan.genomics.cn/ucdisk/s/B7Z3mm.

Competing interests

The authors declare that they have no competing interests.

Funding

This work was supported by grants from the National Natural Science Foundation of China (81772016 and 81272177 to XC; 81871522 to PZ) and Open Funding Project of National Key Laboratory of Human Factors Engineering (SYFD150051816K to XL).

Authors' contributions

XC and PZ conceived the study. PZ, LW, HY, XSP, GK and WL carried out the HDBR experiments and collected the samples. JZ and LS performed metabolomics analysis. LP performed the metagenomics analysis. XML performed the transcriptomics analysis. PZ, XC, LS and JZ wrote the manuscript. All authors participated in the interpretation of data. All authors read and approved the final manuscript.

Acknowledgements

We appreciated Ms. Liu Hongju for her help in collecting the samples. We would like to thank Mr. Han Peng, Liu Xingmin, Chen Jianwei, Ji Jingkai, Du Shiyi and Mei Zhanlong for their valuable advice and guidance in analyzing data.

Authors’ information

[1]State Key Laboratory of Space Medicine Fundamentals and Application, China Astronaut Research and Training Center, Beijing 100094, P.R.China

[2]National Key Laboratory of Human Factors Engineering, China Astronaut Research and Training Center, Beijing 100094, P.R.China

[3]BGI-Qingdao, BGI-Shenzhen, Qingdao, 266555, P.R.China

[4]State Key Laboratory of Quality Research in Chinese Medicine, Institute of Chinese Medical Sciences, University of Macau, Macao, P.R.China

[5]MGI, BGI-Shenzhen, Shenzhen 518083, P.R.China

[6]BGI-Shenzhen, Shenzhen 518083, P.R.China

[7]China National GeneBank, BGI-Shenzhen, Shenzhen 518120, P.R.China

References

1. Chen JW, Ni BB, Li B, Yang YH, Jiang SD, Jiang LS: The responses of autophagy and apoptosis to oxidative stress in nucleus pulposus cells: implications for disc degeneration. *Cellular physiology and biochemistry : international journal of experimental cellular physiology, biochemistry, and pharmacology.* 2014, 34(4):1175-1189.
2. Glasauer S, Mittelstaedt H: Perception of spatial orientation in microgravity. *Brain research Brain research reviews.* 1998, 28(1-2):185-193.
3. Cappellesso R, Nicole L, Guido A, Pizzol D: Spaceflight osteoporosis: current state and future perspective. *Endocrine regulations.* 2015, 49(4):231-239.
4. Fitts RH, Riley DR, Widrick JJ: Physiology of a microgravity environment invited review: microgravity and skeletal muscle. *J Appl Physiol (1985).* 2000, 89(2):823-839.
5. Hughson RL, Helm A, Durante M: Heart in space: effect of the extraterrestrial environment on the cardiovascular system. *Nature reviews Cardiology.* 2018, 15(3):167-180.
6. Garrett-Bakelman FE, Darshi M, Green SJ, Gur RC, Lin L, Macias BR, McKenna MJ, Meydan C, Mishra T, Nasrini J *et al*: The NASA Twins Study: A multidimensional analysis of a year-long human spaceflight. *Science.* 2019, 364(6436).
7. Grabherr L, Mast FW: Effects of microgravity on cognition: The case of mental imagery. *Journal of vestibular research : equilibrium & orientation.* 2010, 20(1):53-60.
8. Crucian BE, Chouker A, Simpson RJ, Mehta S, Marshall G, Smith SM, Zwart SR, Heer M, Ponomarev S, Whitmire A *et al*: Immune System Dysregulation During Spaceflight: Potential Countermeasures for Deep Space Exploration Missions. *Frontiers in immunology.* 2018, 9:1437.
9. Mader TH, Gibson CR, Pass AF, Kramer LA, Lee AG, Fogarty J, Tarver WJ, Dervay JP, Hamilton DR, Sargsyan A *et al*: Optic disc edema, globe flattening, choroidal folds, and hyperopic shifts observed in astronauts after long-duration space flight. *Ophthalmology.* 2011, 118(10):2058-2069.
10. Marshall-Goebel K, Laurie SS, Alferova IV, Arbeille P, Aunon-Chancellor SM, Ebert DJ, Lee SMC, Macias BR, Martin DS, Pattarini JM *et al*: Assessment of Jugular Venous Blood Flow Stasis and Thrombosis During Spaceflight. *JAMA network open.* 2019, 2(11):e1915011.
11. Singh KP, Kumari R, Dumond JW: Simulated microgravity-induced epigenetic changes in human lymphocytes. *Journal of cellular biochemistry.* 2010, 111(1):123-129.
12. Gambara G, Salanova M, Ciciliot S, Furlan S, Gutsmann M, Schiffl G, Ungethuem U, Volpe P, Gunga HC, Blottner D: Microgravity-Induced Transcriptome Adaptation in Mouse Paraspinal longissimus dorsi Muscle Highlights Insulin Resistance-Linked Genes. *Frontiers in physiology.* 2017, 8:279.
13. Michaletti A, Gioia M, Tarantino U, Zolla L: Effects of microgravity on osteoblast mitochondria: a proteomic and metabolomics profile. *Scientific reports.* 2017, 7(1):15376.
14. Sun YV, Hu YJ: Integrative Analysis of Multi-omics Data for Discovery and Functional Studies of Complex Human Diseases. *Advances in genetics.* 2016, 93:147-190.

15. Corfield AP: The Interaction of the Gut Microbiota with the Mucus Barrier in Health and Disease in Human. *Microorganisms.* 2018, 6(3).
16. Feng Q, Chen WD, Wang YD: Gut Microbiota: An Integral Moderator in Health and Disease. *Frontiers in microbiology.* 2018, 9:151.
17. Jiang P, Green SJ, Chlipala GE, Turek FW, Vitaterna MH: Reproducible changes in the gut microbiome suggest a shift in microbial and host metabolism during spaceflight. *Microbiome.* 2019, 7(1):113.
18. Zhang X, Chu X, Chen L, Fu J, Wang S, Song J, Kan G, Jiang W, He G, Chen X *et al*: Simulated weightlessness procedure, head-down bed rest impairs adult neurogenesis in the hippocampus of rhesus macaque. *Molecular brain.* 2019, 12(1):46.
19. Fitts RH, Bodine SC, Romatowski JG, Widrick JJ: Velocity, force, power, and Ca2+ sensitivity of fast and slow monkey skeletal muscle fibers. *J Appl Physiol (1985).* 1998, 84(5):1776-1787.
20. Chen Y, Chen Y, Shi C, Huang Z, Zhang Y, Li S, Li Y, Ye J, Yu C, Li Z *et al*: SOAPnuke: a MapReduce acceleration-supported software for integrated quality control and preprocessing of high-throughput sequencing data. *GigaScience* 2018, 7(1):1-6.
21. Kim D, Langmead B, Salzberg SL: HISAT: a fast spliced aligner with low memory requirements. *Nature methods.* 2015, 12(4):357-360.
22. Love MI, Huber W, Anders S: Moderated estimation of fold change and dispersion for RNA-seq data with DESeq2. *Genome biology.* 2014, 15(12):550.
23. Wen B, Mei Z, Zeng C, Liu S: metaX: a flexible and comprehensive software for processing metabolomics data. *BMC bioinformatics.* 2017, 18(1):183.
24. Wishart DS, Jewison T, Guo AC, Wilson M, Knox C, Liu Y, Djoumbou Y, Mandal R, Aziat F, Dong E *et al*: HMDB 3.0--The Human Metabolome Database in 2013. *Nucleic acids research.* 2013, 41(Database issue):D801-807.
25. Langfelder P, Horvath S: WGCNA: an R package for weighted correlation network analysis. *BMC bioinformatics.* 2008, 9:559.
26. Nurk S, Meleshko D, Korobeynikov A, Pevzner PA: metaSPAdes: a new versatile metagenomic assembler. *Genome research.* 2017, 27(5):824-834.
27. Besemer J, Borodovsky M: GeneMark: web software for gene finding in prokaryotes, eukaryotes and viruses. *Nucleic acids research.* 2005, 33(Web Server issue):W451-454.
28. Huang Y, Niu B, Gao Y, Fu L, Li W: CD-HIT Suite: a web server for clustering and comparing biological sequences. *Bioinformatics (Oxford, England).* 2010, 26(5):680-682.
29. Sun J: CARMA3: A novel scaffold protein in regulation of NF-κB activation and diseases. *World journal of biological chemistry.* 2010, 1(12):353-361.
30. Li R, Yu C, Li Y, Lam TW, Yiu SM, Kristiansen K, Wang J: SOAP2: an improved ultrafast tool for short read alignment. *Bioinformatics (Oxford, England).* 2009, 25(15):1966-1967.
31. Luo H, Wang C, Feng M, Zhao Y: Microgravity inhibits resting T cell immunity in an exposure time-dependent manner. *International journal of medical sciences.* 2014, 11(1):87-96.

32. Koh A, De Vadder F, Kovatcheva-Datchary P, Backhed F: From Dietary Fiber to Host Physiology: Short-Chain Fatty Acids as Key Bacterial Metabolites. *Cell.* 2016, 165(6):1332-1345.
33. Arpaia N, Campbell C, Fan X, Dikiy S, van der Veeken J, deRoos P, Liu H, Cross JR, Pfeffer K, Coffer PJ *et al*: Metabolites produced by commensal bacteria promote peripheral regulatory T-cell generation. *Nature.* 2013, 504(7480):451-455.
34. Chen J, Vitetta L: The Role of Butyrate in Attenuating Pathobiont-Induced Hyperinflammation. *Immune network.* 2020, 20(2):e15.
35. Walsh ME, Bhattacharya A, Sataranatarajan K, Qaisar R, Sloane L, Rahman MM, Kinter M, Van Remmen H: The histone deacetylase inhibitor butyrate improves metabolism and reduces muscle atrophy during aging. *Aging cell.* 2015, 14(6):957-970.
36. Jin M, Zhang H, Zhao K, Xu C, Shao D, Huang Q, Shi J, Yang H: Responses of Intestinal Mucosal Barrier Functions of Rats to Simulated Weightlessness. *Frontiers in physiology.* 2018, 9:729.
37. Cervantes JL, Hong BY: Dysbiosis and Immune Dysregulation in Outer Space. *International reviews of immunology.* 2016, 35(1):67-82.
38. Spencer SP, Fragiadakis GK, Sonnenburg JL: Pursuing Human-Relevant Gut Microbiota-Immune Interactions. *Immunity.* 2019, 51(2):225-239.
39. Zheng D, Liwinski T, Elinav E: Interaction between microbiota and immunity in health and disease. *Cell research.* 2020, 30(6):492-506.
40. Luu M, Weigand K, Wedi F, Breidenbend C, Leister H, Pautz S, Adhikary T, Visekruna A: Regulation of the effector function of CD8(+) T cells by gut microbiota-derived metabolite butyrate. *Scientific reports.* 2018, 8(1):14430.
41. Bengoechea JA, Sa Pessoa J: Klebsiella pneumoniae infection biology: living to counteract host defences. *FEMS microbiology reviews.* 2019, 43(2):123-144.
42. Sarria JC, Vidal AM, Kimbrough RC, 3rd: Infections caused by Kluyvera species in humans. *Clinical infectious diseases : an official publication of the Infectious Diseases Society of America.* 2001, 33(7):E69-74.
43. Ticinesi A, Nouvenne A, Cerundolo N, Catania P, Prati B, Tana C, Meschi T: Gut Microbiota, Muscle Mass and Function in Aging: A Focus on Physical Frailty and Sarcopenia. *Nutrients.* 2019, 11(7).
44. Wu CS, Wei Q, Wang H, Kim DM, Balderas M, Wu G, Lawler J, Safe S, Guo S, Devaraj S *et al*: Protective Effects of Ghrelin on Fasting-Induced Muscle Atrophy in Aging Mice. *The journals of gerontology Series A, Biological sciences and medical sciences.* 2020, 75(4):621-630.
45. Hatter JA, Kouche YM, Melchor SJ, Ng K, Bouley DM, Boothroyd JC, Ewald SE: Toxoplasma gondii infection triggers chronic cachexia and sustained commensal dysbiosis in mice. *PloS one.* 2018, 13(10):e0204895.
46. Jackson MA, Jeffery IB, Beaumont M, Bell JT, Clark AG, Ley RE, O'Toole PW, Spector TD, Steves CJ: Signatures of early frailty in the gut microbiota. *Genome medicine.* 2016, 8(1):8.

47. Varian BJ, Gourishetti S, Poutahidis T, Lakritz JR, Levkovich T, Kwok C, Teliousis K, Ibrahim YM, Mirabal S, Erdman SE: Beneficial bacteria inhibit cachexia. *Oncotarget.* 2016, 7(11):11803-11816.
48. Bindels LB, Beck R, Schakman O, Martin JC, De Backer F, Sohet FM, Dewulf EM, Pachikian BD, Neyrinck AM, Thissen JP *et al*: Restoring specific lactobacilli levels decreases inflammation and muscle atrophy markers in an acute leukemia mouse model. *PloS one.* 2012, 7(6):e37971.
49. Munukka E, Rintala A, Toivonen R, Nylund M, Yang B, Takanen A, Hanninen A, Vuopio J, Huovinen P, Jalkanen S *et al*: Faecalibacterium prausnitzii treatment improves hepatic health and reduces adipose tissue inflammation in high-fat fed mice. *The ISME journal.* 2017, 11(7):1667-1679.
50. Enoki Y, Watanabe H, Arake R, Sugimoto R, Imafuku T, Tominaga Y, Ishima Y, Kotani S, Nakajima M, Tanaka M *et al*: Indoxyl sulfate potentiates skeletal muscle atrophy by inducing the oxidative stress-mediated expression of myostatin and atrogin-1. *Scientific reports.* 2016, 6:32084.

Figures

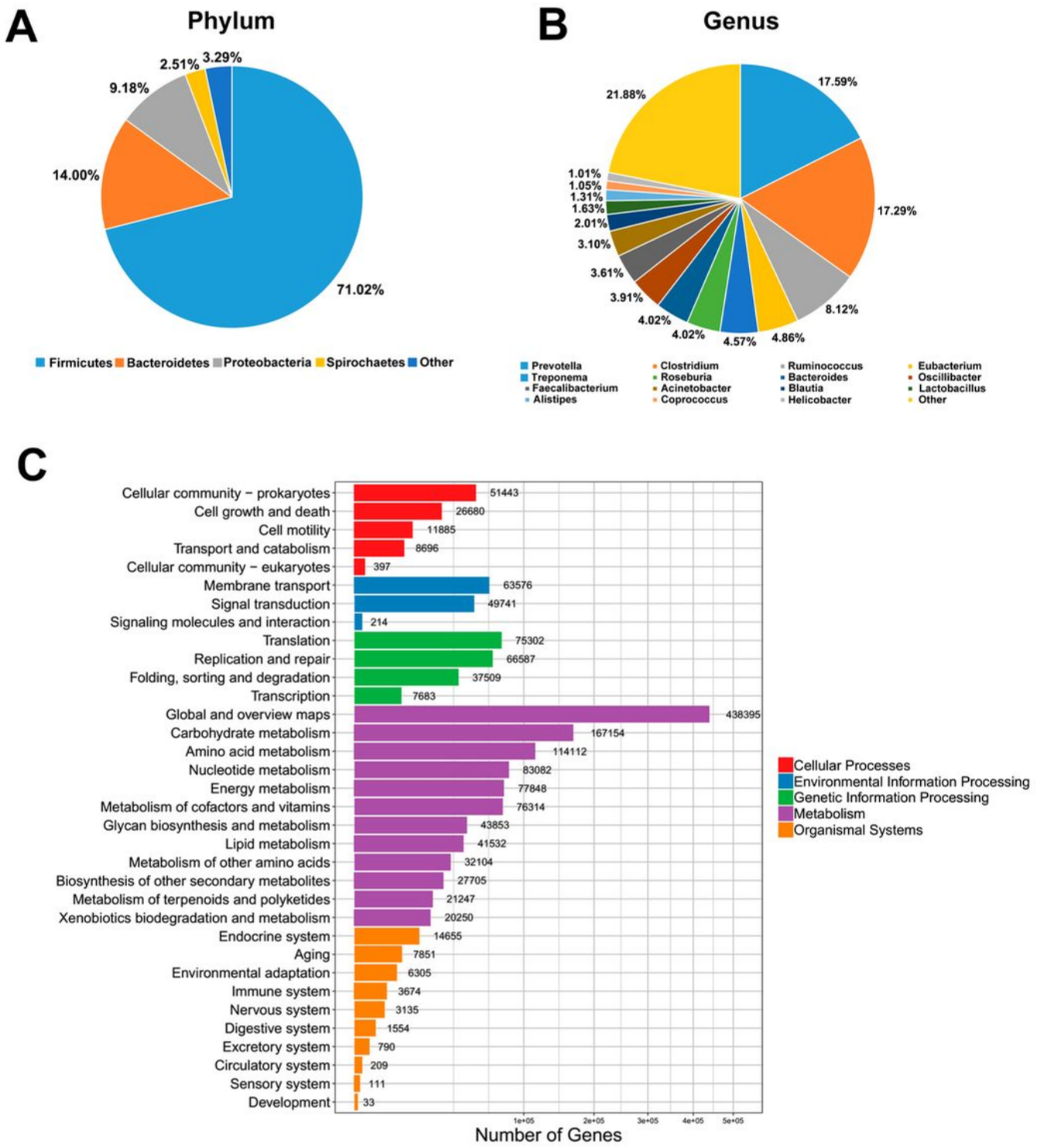

Figure 1

Taxonomic annotation of the 3.2 Mb rhesus macaque intestinal microbiota gene catalog. (A) Top 5 abundant phyla. (B) Top 16 abundant genera. (C) KEGG functional categories of DEGs associated with HDBR; x and y axes show the number of genes and KEGG pathways, respectively.

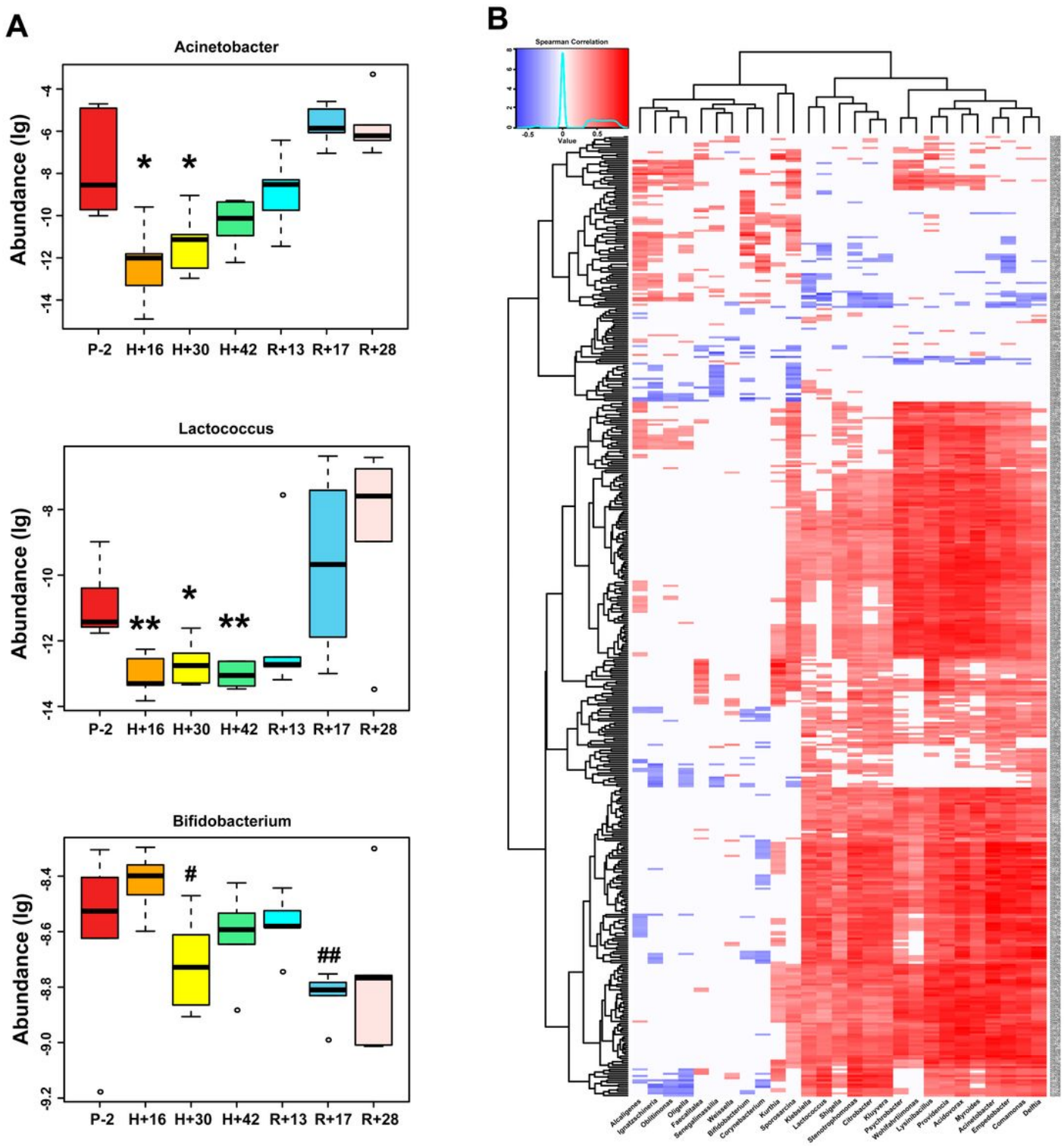

Figure 2

Representative gut bacteria altered by HDBR and association of differentially abundant bacterial genera with differentially represented KOs. (A) Boxplots of the abundance of Acinetobacter, Lactococcus, and Bifidobacterium. The x and y axes show different time points and abundance (log10) of each genera, respectively. For each interquartile range (IQR), the first and third quartiles are shown as boxes and the line inside the box is the median. Data points (circles) outside of the whiskers are the lowest or highest

values within 1.5 times the IQR. *P<0.05, **P<0.01 compared with P-2 by Wilcoxon test; #P<0.05, ##P<0.01 compared with H+16 by Wilcoxon test. (B) Spearman correlation coefficient heatmap (P<0.05) of 27 differentially abundant genera (x axis) and 442 differentially represented KOs (y axis). Red and blue represent significantly positive and negative correlations, respectively, and blank areas indicate that there is no significant correlation.

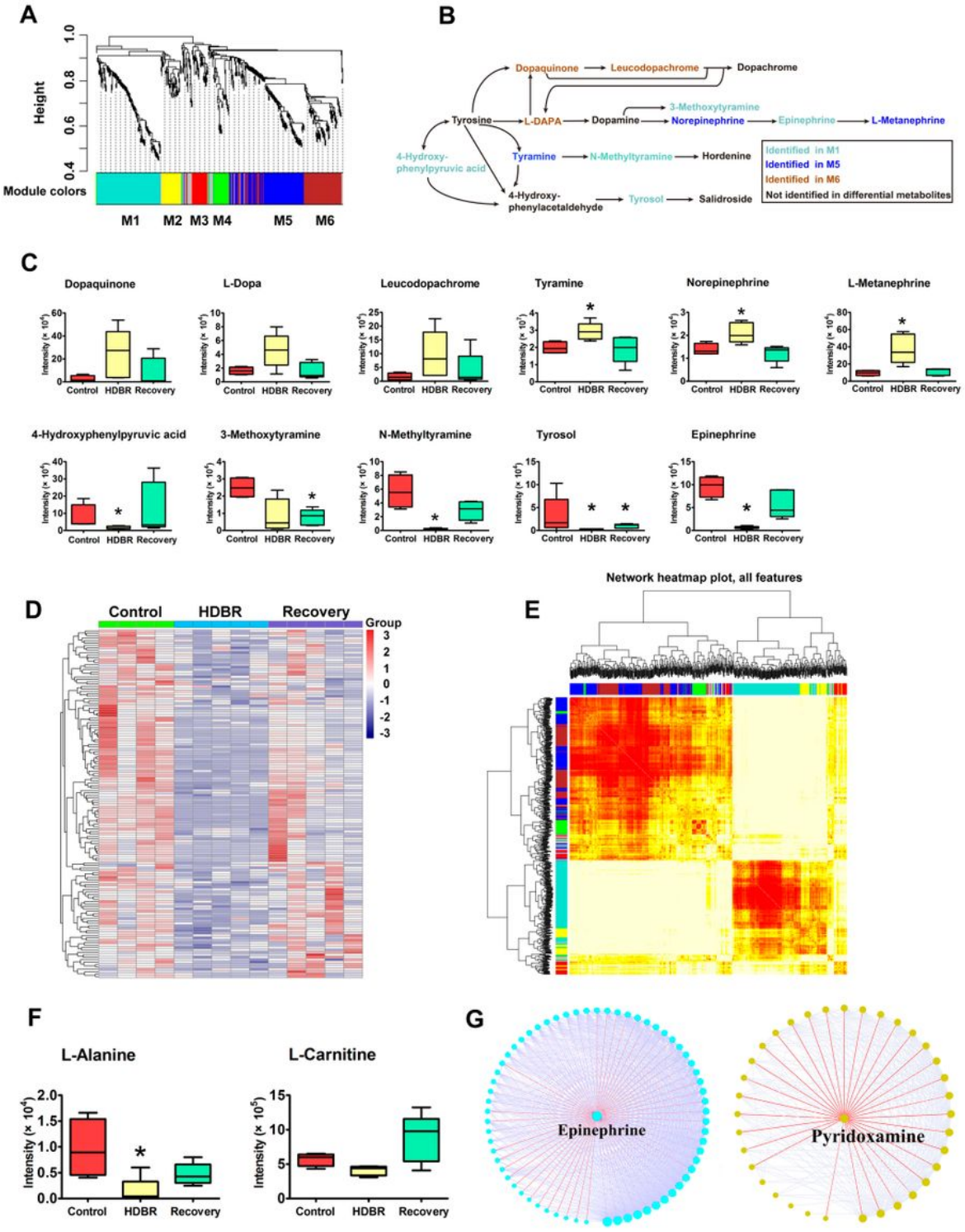

Figure 3

WGCNA of metabolites in atrophied muscle caused by HDBR. (A) Dendrogram of 552 muscle DAFs clustering into 6 modules (M1–M6 colored turquoise, yellow, red, green, blue, and brown; the gray module includes DAFs that did not meet the clustering criteria). (B) Significantly altered metabolites involved in the tyrosine metabolism pathway. Five metabolites in M1 that decreased in abundance during HDBR and increased during recovery are colored in turquoise; 3 metabolites in M5 showing the opposite change are colored in blue; and 3 metabolites in M6 showing a similar change to M1 are colored in brown. The 5 remaining metabolites colored in gray did not show differential abundance. (C). Abundance of metabolites shown in Figure 2B. *P<0.05 vs control group. (D) Heatmap of DAFs in M1 downregulated during HDBR and upregulated during recovery in muscle. (E) Correlation of all muscle DAFs in M1 showing good similarity. M1–M6 are colored as in panel A. (F) Abundance of L-alanine and L-carnitine in HDBR-induced muscle atrophy. *P<0.05 vs control group. (G) Epinephrine and pyridoxamine were identified as hub metabolite for M1 and M6, respectively. Correlations of M1 and M6 DAFs were calculated by WGCNA; a larger node size indicates a greater number of neighbors for the node.

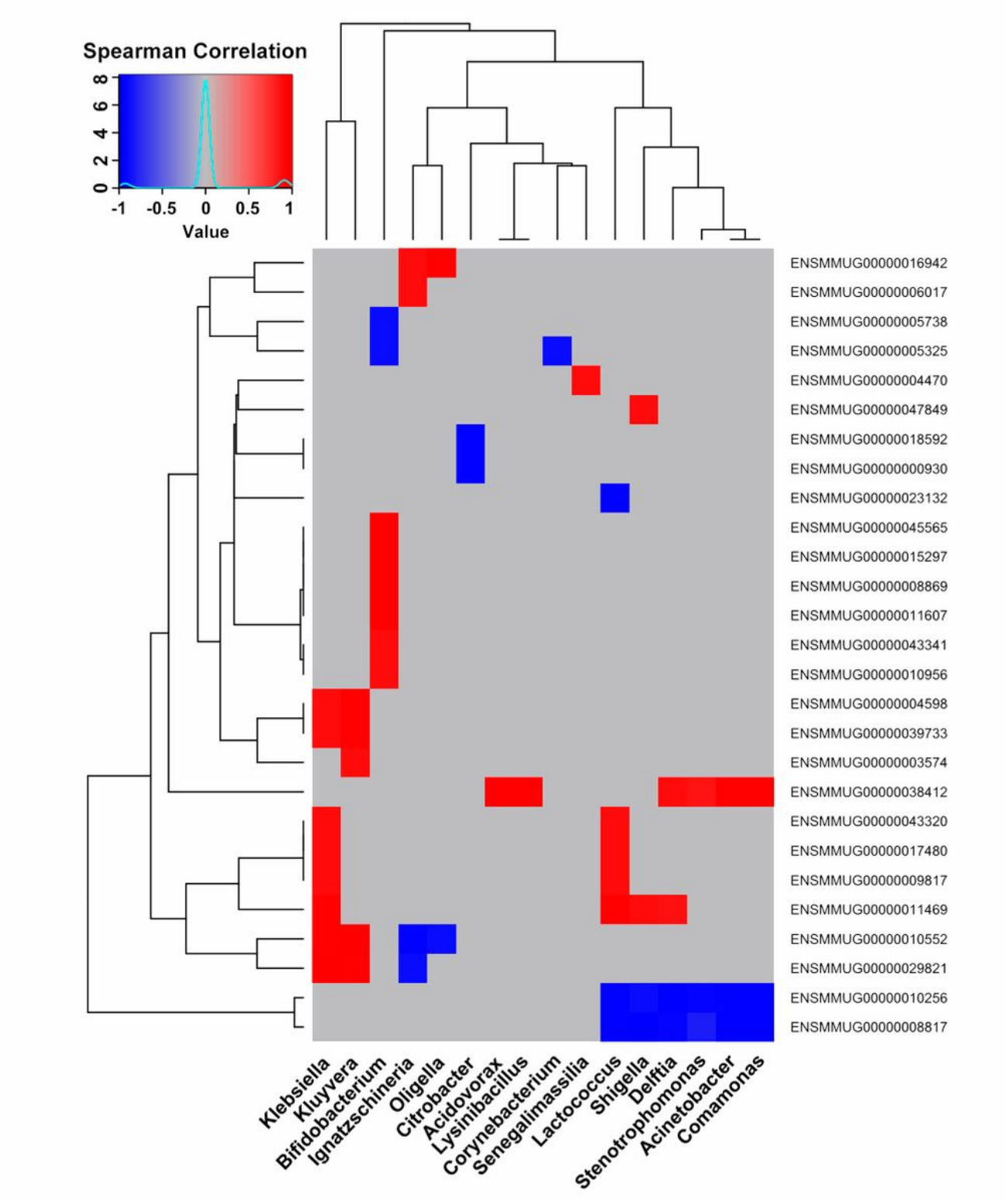

Figure 4

Spearman's rank correlations between differentially abundant intestinal bacteria and DEGs in PBMCs during HDBR. The x and y axes show the 16 genera and 27 DEGs that were significantly correlated (R2>0 and P<0.05). Red and blue colors represent positive and negative correlations, respectively, and gray indicates that there is no significant correlation.

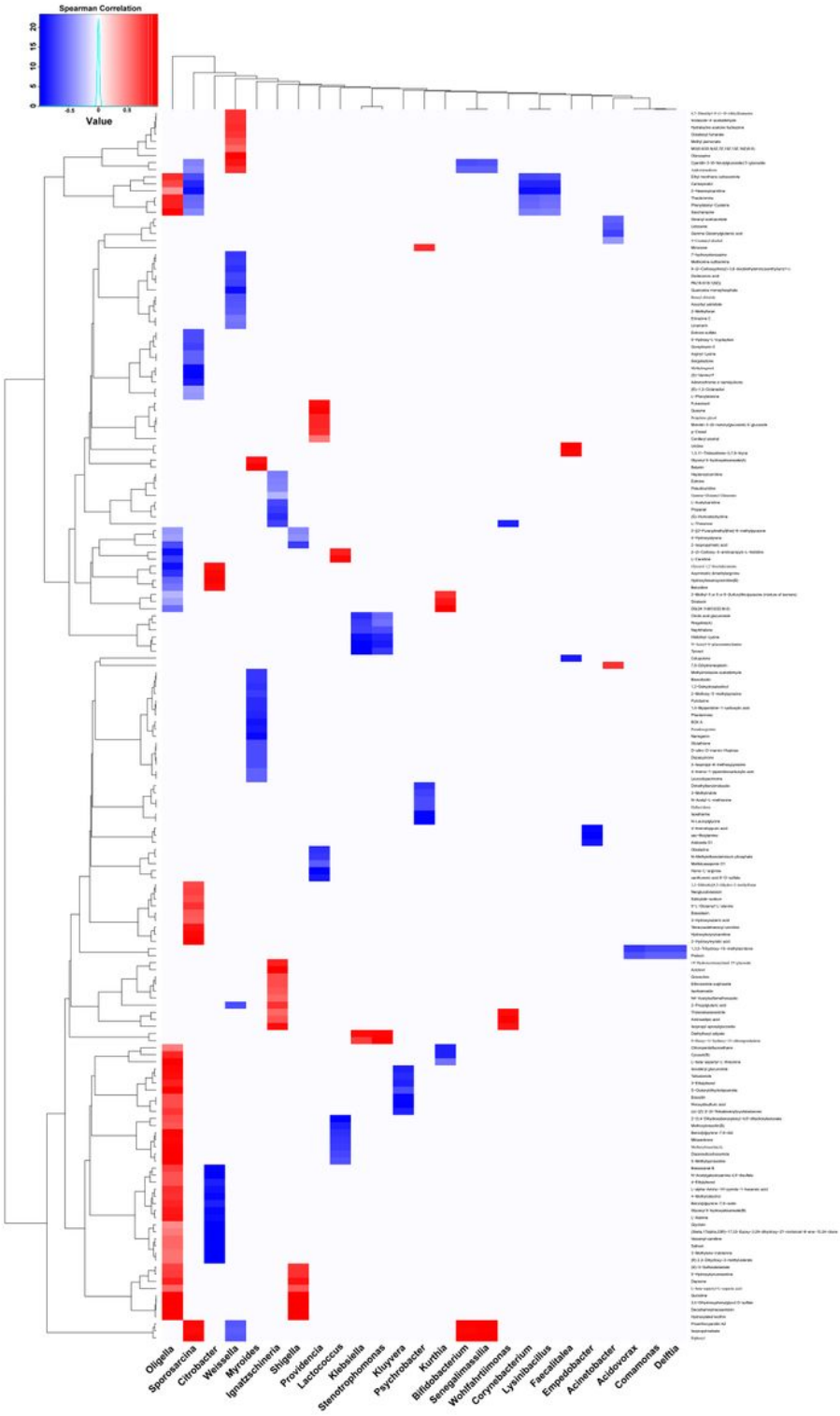

Figure 5

Spearman's rank correlation between differentially abundant intestinal bacteria and metabolites in muscle. The x and y axes represent 25 genera and 174 metabolites with significant correlations (R2>0 and P<0.05). Red and blue represent positive and negative correlations, respectively, and white indicates that there is no significant correlation.

Supplementary Files

This is a list of supplementary files associated with this preprint. Click to download.

- FigureS1.jpg
- FigureS2.jpg
- FigureS3.jpg
- FigureS4.jpg
- FigureS5.jpg
- TableS1.docx
- TableS2.docx
- TableS3.docx
- TableS4.docx
- TableS5.docx
- TableS6.docx
- TableS7.xlsx